Published in final edited form as:

Cancer Res. 2021 August 15; 81(16): 4230–4241. doi:10.1158/0008-5472.CAN-20-3625.

An AIB1 isoform alters enhancer access and enables progression of early stage triple-negative breast cancer

Ghada M Sharif[1], **Moray J Campbell**[2], **Apsra Nasir**[1], **Surojeet Sengupta**[3], **Garrett T Graham**[1], **Max H Kushner**[1], **William B Kietzman**[1], **Marcel O Schmidt**[1], **Gray W Pearson**[1], **Olivier Loudig**[4], **Susan Fineberg**[5], **Anton Wellstein**[1], **Anna T. Riegel**[1,*]

[1]Lombardi Comprehensive Cancer Center, Georgetown University Medial Center, Washington, DC 20057

[2]Division of Pharmaceutics and Pharmaceutical Chemistry, College of Pharmacy, 442 Riffe Building, The Ohio State University, Columbus, OH 4321

[3] The Hormel Institute,University of Minnesota, Medical Research Center, 801 16th Ave NE, Austin, MN 55912

[4]Hackensack Meridian Health Center for Discovery and Innovation, Nutley, NJ 07110

[5]Department of Pathology, Albert Einstein College of Medicine of Yeshiva University, Bronx, NY 10461

Abstract

AIB1Δ4 is an N-terminally truncated isoform of the oncogene Amplified In Breast Cancer 1 (AIB1) with increased expression in high-grade human ductal carcinoma in situ (DCIS). However, the role of AIB1Δ4 in DCIS malignant progression has not been defined. Here we CRISPR-engineered RNA splice junctions to produce normal and early stage DCIS breast epithelial cells that expressed only AIB1Δ4. These cells showed enhanced motility and invasion in 3D cell culture. In zebrafish, AIB1Δ4-expressing cells enabled invasion of parental cells when present in a mixed population. In mouse xenografts, a subpopulation of AIB1Δ4 cells mixed with parental cells enhanced tumor growth, recurrence, and lung metastasis. AIB1Δ4 ChIP-seq revealed enhanced binding to regions including peroxisome proliferator activated receptor (PPAR) and glucocorticoid receptor (GR) genomic recognition sites. H3K27ac and H3K4me1 genomic engagement patterns revealed selective activation of breast cancer-specific enhancer sites by AIB1Δ4. AIB1Δ4 cells displayed upregulated inflammatory response genes and downregulated PPAR signaling gene expression patterns. In the presence of AIB1Δ4 enabler cells, parental cells increased NFκB and WNT signaling. Cellular crosstalk was inhibited by the PPARγ agonist efatutazone but was enhanced by treatment with the GR agonist dexamethasone. In conclusion, expression of the AIB1Δ4-selective cistrome in a small subpopulation of cells triggers an “enabler” phenotype

* Correspondence: Anna T. Riegel, Georgetown University, 3970 Reservoir Rd NW, NRB E307, Washington, DC 20007. Ph: (202) 687-1479. ariege01@georgetown.edu.

Author contributions

Conceptualization and Methodology, GMS, AW and ATR; Investigation, GMS, AN, OL, SF and SS; Formal Analysis, GMS and MJC; Data Curation, MJC, GMS and GTG; Writing – Original Draft, GMS, ATR and MJC; Writing – Review & Editing, GMS, MJC, MHK, WBK, GTG, MOS, GWP, OL, SF, AW, and ATR; Funding Acquisition, ATR, AW and GWP.

The authors declare no potential conflicts of interest.

hallmarked by an invasive transcriptional program and collective malignant progression in a heterogeneous tumor population.

Keywords

Amplified in breast cancer 1 (AIB1); AIB1Δ4; CRISPR; Splicing Isoform; Progression

INTRODUCTION

Greater depth and read-length of RNA sequencing has revealed a large number of alternatively spliced transcripts in human cancers that may directly contribute to the oncogenic process and offer novel therapeutic possibilities (1,2). Altered ratios of alternatively spliced transcripts have been linked to tumor initiation and progression (3), different cancer stages (4) and therapy resistance (5) although it has been difficult to dissect distinct functions of each gene isoform in isolation. Here we show that CRISPR targeting can be used to reveal unique enabler functions of a splice isoform of a transcriptional coactivator, AIB1.

AIB1 (Amplified In Breast Cancer 1), also known as nuclear receptor coactivator 3 (NCOA3) or steroid receptor coactivator 3 (SRC-3) was identified due to its amplification and/or over-expression in breast and other cancers(6–8). AIB1 is an oncogene in several model systems of xenografts and transgenic mice (9–14). In addition to coactivating transcription of hormone receptors such as estrogen and progesterone receptor (ER, PR), AIB1 can also drive malignancy and invasion in the ER and PR negative setting via several other transcription factors such as AP-1, TEADs, E2Fs, ETS and NFκB (11,15). We reported an mRNA splice isoform known as AIB1Δ4, which is expressed in cancer cells along with full length AIB1 in most cell types examined. The AIB1Δ4 protein is missing the first 223 amino acids from the N-terminus of the protein containing the PAS-HLH domains (16,17). This truncation is due to an alternative splicing event where exon 4 is skipped leading to a new translation start site on exon 7 in frame with the full length AIB1 isoform (16). AIB1Δ4 shows low to undetectable expression in normal human mammary epithelium, but is upregulated in early stage breast cancers (DCIS) and further increased in breast cancer cell lines that metastasize to the lung, brain and bone and in pancreatic cancer cell lines that metastasize to the liver and spleen (16). In mice, AIB1Δ4 overexpression in the presence of endogenous AIB1 induced ectasia and increased mammary epithelial cell proliferation via upregulation of cyclin D1 and IGF-I receptor signaling (18) all of which are also activated by AIB1 full length overexpression (8). When overexpressed against a background of the full length AIB1 *in vitro*, AIB1Δ4 can increase activation of nuclear receptors, NFκB and transcription factors involved in epidermal growth factor (EGF) induced transcription (17–19). The increased activity of the AIB1Δ4 isoform has been attributed in part to the lack of an inhibitory domain on the missing N-terminus in AIB1Δ4 that binds the tumor suppressor ANCO1/ANKRD11 (20,21). However, in all functional *in vitro* and *in vivo* studies to date, AIB1Δ4 effects have been gauged by overexpression in the presence of full length endogenous AIB1 or in knock down approaches where both AIB1 isoforms (full length and Δ4) were depleted. Thus it has been impossible to discern whether there are distinct

functions of AIB1Δ4, or whether it interacts with overlapping genomic loci and the same transcription regulatory elements as full length AIB1.

Here we evaluated the function of the AIB1Δ4 isoform in the progression of early stage breast cancer using the triple negative (ER-/PR-/HER2-) MCFDCIS cells which is the most widely-used model of human early stage breast cancer progression (22,23). Triple negative (TN) DCIS is detected in about 5–10 % of cases and TN DCIS lesions are thought to rapidly progress to high grade DCIS and invasive breast cancer (24,25). We show that AIB1Δ4 is increased in high grade DCIS tissue. Using CRISPR-based genome editing, we derived normal MCF10A (26) and MCFDCIS cell lines that only express the AIB1Δ4 isoform and demonstrate that AIB1Δ4 only expressing cells show enhanced invasive and migratory behavior. Most interestingly a small subpopulation of the AIB1Δ4 only expressing cells enabled invasion and metastasis of neighboring parental cells. ChIP-seq of AIB1 isoforms and histone marks revealed significant differences in the isoform-specific cistrome leading to a transcriptome pattern associated with poor outcome in breast cancer.

MATERIALS AND METHODS

Real Time Electric cell impedance sensing (ECIS)

Cell migration, invasion and proliferation were monitored using E- and CIM-plates from xCELLigence, Roche according to the manufacturer's protocol. Human umbilical vein endothelial cells, HUVECs (LONZA, #C-2517A) were used as an endothelial monolayer to monitor cell invasion. Details in the supplementary methods.

3D sphere invasion Assay

Sphere formation assay was conducted as previously described(27). A single cell suspension was embedded in 100% matrigel (Corning, # CB-40230) and spread on the bottom of 8-well chamber arrays (Thermofisher, #154453). Imaged on Olympus IX-71 Inverted epifluorescence microscope. 100–200 spheres per cell line were scored for invasive phenotype. Spheres with 3 or more cells protruding into the extracellular matrix were considered invasive. Graphs show representative data from one of three independent experiments. Aggregates were formed in U-shape 96-well plates (Costar #7007) or 81-well agarose molds from Microtissues (28) then embedded in 20% matrigel: 80% collagen I (Corning # 354236) mix in an 8-well chamber (Thermofisher, #154453). Then imaged using a Zeiss LSM800 microscope. Quantification on mixed spheres was done by counting the number of invading arms with a specific cell type leading the stream of cells. Graphs show representative data from one of three independent experiments. Invasion area quantification was done using ImageJ.

Zebrafish Injection and Imaging

Fifty cells were injected directly into the circulation via the duct of Cuvier of Tg(kdrl:GRCFP)zn1 zebrafish embryos 48 hours post fertilization. Cell extravasation was scored in the tail region in live embryos 48 hours after injection. At the end of the experiments, representative zebrafish embryos from each group were embedded in agarose for still images capture using Zeiss LSM800 microscope.

Animal Experiments

Studies in mice were reviewed and approved by the Georgetown University Animal Care and Use Committee. Animals were randomized to receive control or CRISPR engineered cells. Five hundred thousand cells were injected into the mammary fat pad of six age-matched 8 weeks old female SCID/ Beige mice purchased from Charles River. Two weeks later, all tumors from the right mammary fat pad were removed by survival surgery where tumors from the left mammary fat pad were removed after 5 weeks. A total of 6 mice were injected per condition. Lung metastases were monitored 5–12 weeks post injection using In Vivo Imaging Systems (IVIS Lumina III, Perkin Elmer) machine. In the recurrence experiment, two million cells were injected in the mammary fat pad of 5 NOD/SCID mice, all tumors were removed when they reached the same size (~80cm^2). Xenograft experiments in athymic nude mice (purchased from Invigo) were done by subcutaneously injecting one million cells in each flank.

ChIP-Seq

Cells were crosslinked using 1.2% formaldehyde for 10 minutes at room temperature, stopped by 2M glycine for 5 minutes at room temperature. Cells were collected in 1X PBS containing protease and phosphatase inhibitors (Sigma, #4693159001, # 4906837001) and 10mM DTT. The nuclei were isolated sonicated using Bioruptor plus™ (Diagenode Inc., Denville, NJ). Pre-cleared lysates were mixed with protein A magnetic beads bound to AIB1 (Cell signaling, #2126, RRID:AB_823642), H3K4me1 (Active motif, #39297, RRID:AB_2615075) or H3K27ac (Active motif, #39135, RRID:AB_2614979) antibodiesovernight at 4°C. Samples were de-crosslinking at 65°C in the presence of 200mM NaCl and proteinase K. QIAquick PCR purification kit was used to isolate the DNA fragments. DNA sequencing libraries were prepared using the Kapa Hyper DNA library prep (Roche). For AIB1 ChIP-seq, we used low cell ChIP-seq kit (active Motif # 53084) to isolate chromatin complexes and purify DNA fragments.

All samples were prepared in biological triplicates. ChIP-Seq data were aligned to hg19 using Rsubread (29) and the differential genomic binding was established using csaw(30). Peaks were annotated to genes within indicated distances to genomic features using the annotatePeakInBatch function from ChIPpeakAnno (RRID:SCR_012828). Motif enrichment in peaks was undertaken using the findMotifsGenome.pl tool available from the *HOMER* (Hypergeometric Optimization of Motif EnRichment, *RRID:SCR_010881*) (31).

RNA-Seq, GSEA and IPA

Biological triplicate samples per experimental condition were analyzed, raw sequence reads (75bp paired end, >45×10^6 average reads/sample) were aligned to the human genome (hg19) using Rsubread, and aligned reads translated to expression counts via featurecounts, followed by a standard edgeR (RRID:SCR_012802) pipeline to identify DEGs under specific conditions. Gene set enrichment analysis (GSEA, RRID:SCR_003199) of BROAD Hallmark pathways was done using a list of all differentially expressed genes ranked by signed log10(FDR). Hallmark gene sets were filtered by NES > 1.5, FDR q-value < 0.05. GSEA and Ingenuity pathway analysis (IPA, RRID:SCR_008653) was undertaken using a list of all differentially expressed genes to identify canonical pathways.

Phospho-Kinase profiler

DCIS cells starved overnight. Next day, 20% DCIS-Δ4 cells were added to the DCIS cells for 0 or 30min. Cell lysates were prepared and blotted on the Human Phospho-kinase array (R&D, #ARC003C) according to the manufacturer's protocol. Membranes were imaged using an ImageQuant™ LAS 4000 biomolecular imager (GE) and signal intensity was quantified using ImageJ, RRID:SCR_003070.

Statistics

Analyses were undertaken either using the R platform for statistical computing (version 3.6.1) and the indicated library packages implemented in Bioconductor (RRID:SCR_006442) or Prism 7 (Graphpad Inc, RRID:SCR_006442). Analysis of variance was used for multiple comparisons and t-tests were used for paired comparisons, with $p<0.05$ as the threshold for statistical significance in all tests. Kaplan–Meier plots were generated from publicly available data sets at http://kmplot.com/analysis. The top ~50 up- and downregulated genes in DCIS-Δ4 and 10A-Δ4 cells compared to parental cells were used to establish an AIB1Δ4 signature profile. Using the "Use multiple genes" option, genes were equally weighted and downregulated genes were inverted to represent directionality of regulation. Relapse-free and overall survival analyses were run on datasets from patients with estrogen-negative tumors.

Data Availability

The RNA-sequencing data have been deposited to the Gene Expression Omnibus under record GSE139270. The AIB1 and histone marks ChIP-sequencing data have been deposited to the Gene Expression Omnibus under record GSE144632 and GSE139367, respectively. AIB1 ChIP-seq dataset in MCF7 was obtained from Zwart el al (32) at http://www.carroll-lab.org.uk/data.

RESULTS

The AIB1Δ4 splice variant enhances cell motility and invasion.

To compare AIB1Δ4 expression levels in low and high grade DCIS samples we analyzed formalin fixed and paraffin embedded (FFPE) using isoform specific primers that were optimized to detect short RNA fragments isolated from FFPE samples (33). High grade DCIS samples had significantly higher AIB1Δ4 expression (Fig. 1A) suggesting a possibly distinct role for AIB1Δ4 during malignant progression.

To study the contribution of AIB1Δ4 to breast cancer malignant progression we utilized the immortalized normal human mammary epithelial MCF10A cells (26) and their derivative early stage breast cancer MCFDCIS cells (22). Previous studies have shown that pan AIB1 knockdown in MCFDCIS is associated with reduced DCIS lesion formation and progression (12). We generated isogenic cell lines expressing AIB1Δ4 and not the full length AIB1 using CRISPR editing of the exon 4 splice acceptor site (Fig. 1B). This editing resulted in deletions in the exon 3, intron 3 and exon 4 region (Fig. 1C and S1A) as detected at the mRNA level in the MCFDCIS and the MCF10A cell lines (Fig. 1D, S1B and S1C). The resulting cell lines were designated DCIS-Δ4 and 10A-Δ4, respectively. CRISPR editing of

exon 4 resulted in the loss of the 160 kDa full length AIB1 protein but not the 140 kDa AIB1Δ4 isoform (Fig. 1E and S1D) that is detectable predominantly in the nucleus of the engineered lines similar to full length AIB1 (Fig. 1F). We obtained an additional MCFDCIS derived clone (DCIS-Δ4-hy) that expresses low but detectable levels of full length AIB1 (Fig. S1C and S1D). It shows a larger genomic deletion that includes both exon 3 and 4 (Fig. S1A) and two dominant transcripts; both of which are missing exon 4 (Fig. S1B and S1C). This hypomorph line expresses detectable full length AIB1, presumably from the non-CRISPR allele and is useful in experiments to confirm effects of an increased relative expression of AIB1Δ4.

The DCIS-Δ4 and 10A-Δ4 cell lines have altered morphology (Fig. 1F) and increased motility and migration rate when plated in the top chamber of a transwell migration assay using real-time Electric Cell Impedance Sensing (ECIS) (Fig. 1G and S1E) (34,35). They also have enhanced endothelial monolayer disruption compared to controls (Fig. 1H) in a transendothelial invasion assay (Fig. S1E). DCIS-Δ4-hy cells showed enhanced invasive ability similar to the AIB1Δ4 clones (Fig. S1F). Proliferation rates of DCIS-Δ4 cells were unchanged compared to DCIS parental cells. DCIS-Δ4-hy clone showed an increase in proliferation (Fig. S1G and S1H). 10A-Δ4 cells grew slower than their parental counterpart (Fig. S1H) indicating a role for full length AIB1 in normal breast cell proliferation.

Next we studied sphere formation and invasion into extracellular matrix Matrigel™ (27) (see Fig. 1I for schematic). DCIS-Δ4 spheres were comparable in size to the parental DCIS spheres, consistent with equivalent proliferation rates in 2D culture (see Fig. S1H). However, DCIS-Δ4 spheres invaded the surrounding matrix at a significantly higher rate than parental cells (Fig. 1J and 1K). Spheres grown from 10A-Δ4 cells demonstrated an invasive and disorganized phenotype, with individual cells entering into the matrix (Fig. 1J and 1K). The smaller size of 10A-Δ4 relative to the MCF10A spheres is likely due to the slower proliferation rate (see Fig. S1H).

Direct contact with AIB1Δ4 expressing cells enables crosstalk and invasion

To study the impact of expression of AIB1-Δ4 in an early stage breast cancer cell subpopulation we used a 3D invasion assay. Differentially labeled DCIS and DCIS-Δ4 cells were mixed at a 4:1 ratio and embedded in a collagen I / Matrigel™ mix, a medium where invasion can be monitored over time (36) (see Fig. 2A for schematic). DCIS-Δ4 cells were significantly more invasive on their own than their parental counterpart (Fig. 2B) but surprisingly the presence of a minority population of DCIS-Δ4 cells led to enhanced invasion of parental DCIS cells into the surrounding matrix (Fig. 2B). Despite their lower abundance, DCIS-Δ4 cells were seen over two-fold more frequently at the leading edge of the invading stream of cells (Fig. 2C).

We further examined the enabling phenotype in a transgenic zebrafish model (Tg(kdrl: GRCFP)zn1) in which a green reef coral fluorescent protein (GRCFP) is expressed in the vascular endothelia under the control of a VEGFR2 promoter(37). Fluorescently labeled AIB1Δ4 cells were injected alone or in a mixed population directly into the circulation (duct of Couvier) of Zebrafish embryos, and tissue-invading cells scored in the tail region (Fig. 2D). Both DCIS-Δ4 and DCIS-Δ4-hy clones showed a higher invasion rate than an

equivalent number of the parental DCIS cells (Fig. 2E and S2A). DCIS cells in a mixed population with DCIS-Δ4 showed a significantly higher invasion rate than DCIS cells alone (Fig. 2E). In contrast, the 10A-Δ4 cell line showed a low and insignificant change in extravasation rate in zebrafish embryos, probably because they are non-transformed cells(26) (Fig. S2B).

The crosstalk between the DCIS and DCIS-Δ4 cells could be due to an exchange of secreted factors, however there was no effect on invasion when adding conditioned media (CM) from DCIS-Δ4 cells to DCIS cells or DCIS CM to DCIS-Δ4 cells (Fig. S2C). Additionally, in a co-culture migration assay, the DCIS-Δ4 cells enabling effect was not observed on DCIS cells (Fig. S2D and S2E). This suggests that the factor(s) involved are insufficient in CM and a direct cell-cell contact between the parental and AIB1Δ4 cells is needed to initiate the increased invasive effects seen in the mixed population experiments. Indeed, a portion of the enabling effect seems to involve cell-cell contact since DCIS-Δ4 cells efficiently enabled the invasion of DCIS cell when in direct contact, mixed together in the same sphere (see Fig. 2B) but do not affect adjacent DCIS spheres when they are separated (Fig. S2F).

AIB1Δ4 cells *in vivo* are enablers of invasion and metastasis

To determine if the DCIS-Δ4 cell enabler effect occurred in tumors, we injected 500,000 parental DCIS or DCIS-Δ4 cells into the mammary fat pad of immune compromised SCID/Beige mice. Mixing DCIS-Δ4 cells with the parental DCIS cells at a 1:4 ratio significantly enhanced tumor growth at 5 weeks compared to an equivalent total number of DCIS cells alone (Fig. 3A). Surprisingly the DCIS-Δ4 tumors grew significantly slower than the parental DCIS tumors and presented heterogeneous and less differentiated DCIS lesions (Fig. 3A and S3A). DCIS-Δ4-hy tumors grew larger than DCIS tumors (Fig. S3B) paralleling their increased *in vitro* proliferation rate (see Fig. S1G). We examined the spatial expression of P63 in DCIS lesions using an antibody that can recognize both human and mouse P63 to detect both luminal epithelial (xenograft) and myoepithelial (mouse) cells. P63 expression loss in the myoepithelial layer is an indicator of early transition to an invasive state whereas the gain of P63 expression in tumor epithelial cells marks a basal-like phenotype and malignant progression (23,38). At week 2, there was a loss of myoepithelial P63 and gain of epithelial P63 in mixed tumors (Fig. 3B). At week 5 an increase in the number of P63 positive luminal epithelial cells was observed (Fig. 3C). Double staining for P63 and Luciferase, (expressed only by MCFDCIS parental cells) in the mixed tumor, showed that the majority are P63 positive cells (Fig. S3C). In DCIS-Δ4-hy tumors, both epithelial p63 and CD44 expression is increased compared to control DCIS tumors (Fig. S3D).

DCIS, DCIS-Δ4 and the mixed tumors were removed via survival surgery at either week 2 or week 5 and peripheral tissues were harvested by week 12 to inspect for metastases. Mice with mixed tumors had a significantly higher incidence of lung metastases (Fig. 3D and S3E) that correlated with the increased size of the primary tumor. Lung metastases were confirmed by qPCR using human specific primers for actin (Fig. 3E) and by IHC staining of luciferase in the parental DCIS cells in the mixed tumors (Fig. 3F). The metastases consisted largely of parental MCFDCIS cells as seen by bioluminescence (Fig. S3E). Presence of

parental cells (Fig. 3F) was confirmed by qPCR of the CRISPR- edited region of the AIB1 gene (Fig. S3F). Thus, MCFDCIS-Δ4 cells appear to enable invasion of neighboring cells yet are not selected as a dominant population that takes over during progression. Consistent with MCFDCIS-Δ4 enabling invasion, tumor recurrence after removal of same-size primary tumors is significantly more rapid in mixed tumors than in DCIS controls (Fig. S3G).

No significant changes in gene expression change were observed in tumors at 2 weeks, and at week 5 there were only 4 significant DEGs related to mitochondrial function and tumor necrosis (Supplementary table S1) These small differences in gene expression are not surprising since the mixed tumors were predominantly composed of parental DCIS cells (Fig. S3H)

Differential genomic engagement of the AIB1Δ4 isoform impacts enhancer accessibility.

To examine if the AIB1Δ4 driven phenotype is related to distinct genomic associations, we performed ChIP-Seq with an AIB1 antibody that binds to the C-terminus of both the full length and the AIB1Δ4 isoforms(21) allowing direct comparison of genomic distribution of chromatin interaction of the isoforms. The total number of peaks observed with AIB1Δ4 is less than AIB1 full length probably due to its lower expression level (see Fig. 1D) but notably 33% of the AIB1Δ4 peaks did not overlap with the AIB1 peaks in the MCFDCIS cell lines (Fig. 4A). Similarly, in MCF10A cells AIB1Δ4 ChIP peaks were distinct (~50%) from AIB1 ChIP peaks (Fig. S4A). AIB1 ChIP seq peaks in an ER positive cell line, MCF7 (32) with and without estradiol (E2) show a distinct distribution on the genome compared to AIB1 and AIB1Δ4 peaks in ER(–) MCFDCIS cells (Fig. S4B) emphasizing the pleiotropic genomic interactions of this coactivator and its isoform in different contexts.

Motif enrichment analyses using HOMER (31) showed that AIB1Δ4 ChIP peaks were uniquely enriched for PPARE, ZNF416 and ZNF189 motifs. Other motifs such as the glucocorticoid receptor element (GRE) were significantly enriched in both isoforms (Fig. 4B). Nuclear receptors interact with the LXXLL motif present in both AIB1 isoforms (15). In MCF10A cells AIB1Δ4 ChIP peaks were exclusively enriched for HIF-1beta, ELF5 and FOXA2 motifs while AP-1 family and TEAD family were significantly enriched in both isoforms (Fig. S4C).

We next examined epigenomic histone marks with ChIP-Seq for H3K27ac and H3K4me1 which associate with chromatin indicating enhancer engagement and activation (39,40). The degree of overlap (at least 1 bp) of histone modifications in the DCIS and DCIS-Δ4 cells (Fig. 4C) was clearly distinct in the two cell backgrounds with only 294 sites in common. H3K27ac peaks also showed a bias towards AIB1Δ4 with 4270 peaks unique to AIB1Δ4 in DCIS-Δ4 cells (Fig. 4C). We overlapped (allowing 500 bp gaps) H3K27ac and H3K4me1 peaks with an enhancer map generated in 47 breast cancer patient samples (BrCa enh.) (41). In DCIS-Δ4 cells, 540 enhancer sites overlapped with H3K27ac/H3K4me1, whereas in full length AIB1 cells only 257 H3K27ac/H3K4me1 sites overlapped with enhancer sites (Fig. 4D and 4E). In normal mammary epithelial cells, H3K27ac/H3K4me1 sites both overlapped with genomic enhancer sites established by the FANTOM5 consortium (hMEC enh.) (42) (Fig. S4D). To reveal the spatial relationship of AIB1 or histone modification enrichment to genes we analyzed the AIB1 peaks or histone modifications in 5kb bins up and down-stream

of transcription start site (TSS) and summed the peaks' scores. The H3K27ac peaks in bins more distal to the TSS trended to be more significant for AIB1Δ4 cells (Fig. S4E). Taken together these data suggest that AIB1Δ4 elevates activation of a specific subset of breast cancer specific enhancers involved in breast cancer progression, in part by increasing the number and significance of H3K27ac sites.

The AIB1Δ4 splice variant regulates a distinct transcriptome

To investigate how the differential genomic binding and increased enhancer accessibility of AIB1Δ4 compared to full length AIB1 impacted gene expression, we performed RNA-Seq on parental MCFDCIS, MCF10A, the AIB1Δ4 derivative lines and their mixed cell populations. Similarity and principal component analyses revealed that experimental conditions explained the majority of variation in expression (Fig. S5A). Consistent with the invasive phenotype presented by DCIS-Δ4 cells, inflammatory response genes and extracellular matrix proteases such as IL1β, MMP9, MMP10, and SERPINB2 were upregulated in the DCIS-Δ4 cell line compared to control as well as genes located on the 1q21.3 cytoband such as SPRR3, S100A7, SPRR2A, IVL, SPRR1A, SPRR2D and LCE3D (Fig. 5A, Supplementary table S1). Gene Set Enrichment Analysis (GSEA) in AIB1Δ4 cells confirmed that NFκB signaling, coagulation and 1q21.3 gene sets were positively enriched compared to parental cells (Fig. 5B); conversely, Myc and E2F targets were down-regulated consistent with the slow growth rate of AIB1Δ4 tumors (Supplementary table S2). From the Ingenuity Pathway Analysis (IPA), the top upregulated pathways were inflammatory response related pathways such as osteoarthritis and toll like receptor signaling (Fig. 5C). Several factors in the coagulation system that function in cell adhesion and spreading as well as cell migration were also regulated. Notably, peroxisome proliferative activated receptor (PPAR) signaling (IPA) and adipogenesis related to PPARγ signaling (GSEA, see Supplementary table S2) were consistently down regulated in AIB1Δ4 expressing cells.

We generated a list of AIB1Δ4 signature genes from the top ~50 up- and downregulated genes in DCIS-Δ4 cells compared to parental DCIS cells. Patients with ER-negative breast tumors and altered expression of these AIB1Δ4 signature genes (Supplementary table S3) had worse relapse-free survival and overall survival outcomes(Fig. S5B). GSEA and IPA analyses of differentially regulated genes in 10A-Δ4 relative to MCF10A cells were also indicative of enhanced inflammatory pathways and invasive transition (Fig. S5C–E and Supplementary table S2). Notably PPAR signaling and cell cycle control pathways were downregulated in the 10A background. AIB1Δ4 regulated genes in MCF10A cells also provided a signature that predicts poor relapse free survival in patients (Fig. S5F and Supplementary table S3).

To uncover the underlying mechanism by which DCIS-Δ4 enables parental DCIS cells invasion, we cultured a mix of 4:1 (DCIS: DCIS-Δ4) cell ratio to allow crosstalk for 48 hours. DCIS and DCIS-Δ4 cells were then separated by flow cytometry and changes in gene expression in each population were analyzed by RNA-Seq. DCIS cells from the mixed population showed an increase in proliferation pathways, such as E2F and Myc targets, consistent with their faster tumor growth *in vivo*. NFκB signaling was positively enriched as well as WNT signaling, the latter associated with DDK1, RAC3 and FOXD1

genes upregulation (Fig. 5D and 5E). A phospho-kinase array confirmed WNT signaling activation in DCIS cells after their coculture with DCIS-Δ4 cells, marked by GSK-3β dephosphorylation and increased WNK1 phosphorylation (43,44) (Fig. 5F). Although WNT signaling has been associated with activation of EMT, changes in EMT markers in DCIS cells were only marginally altered (Fig S5G). Also of note in DCIS cells was down-regulation of PPARγ signaling target genes such as CD36. Interestingly, DCIS-Δ4 cells' gene expression was also impacted by co-culture with DCIS cells showing increase expression of a number of the genes associated with cell adhesion and tumor progression such as fibronectin (FN1) and chondroitin sulfate proteoglycan 4 (CSPG4) (45,46) (Fig. S5H).

Genomic binding and gene expression

To determine the relationship between AIB1 isoform binding strength and gene expression, we used Binding and Expression Target Analysis (BETA)(47). The score of individual peaks for AIB1 or AIB1Δ4 were weighted for distal binding and multiplied by the absolute fold change for a given gene differentially expressed between AIB1 and AIB1Δ4 in DCIS cells. The median top 75th percentile and bottom 25th percentile are shown as a box whisker plot (Fig. 5G). This analysis showed a significant increase in AIB1Δ4 binding at distal regions of regulated genes. The H3K27Ac histone mark was also significantly enriched at regulated genes in the DCIS-Δ4 cell background despite the lower number of overall binding sites of AIB1Δ4 (Fig. 5G).

Blocking the enabler effect of AIB1Δ4 by activating PPARγ signaling pathway

From the gene expression analysis, PPAR signaling and adipogenesis are down regulated in AIB1Δ4 expressing cells (see Fig. 5) and AIB1Δ4 enriched motif analysis (see Fig. 4B) indicates that nuclear receptors such as PPARγ and GR could be involved in the invasive or enabling response. We have previously shown that activation of PPARγ delays ductal carcinoma in situ transition to invasive ductal carcinoma (48). Additionally, PPARγ agonists have been used as anti-inflammatory reagents (49,50). To examine this we used a PPARγ agonist, efatutazone, to investigate PPARγ contribution to the enabler/responder phenotype. While efatutazone had no effect on DCIS-Δ4 cells' invasion, it significantly decreased the enabler/responder phenotype in mixed spheres (Fig. 6A and 6B) suggesting that the PPARγ agonist effect is specific to the crosstalk between DCIS and DCIS-Δ4. We also tested the effect of dexamethasone, a GR agonist, on the enabler / responder crosstalk and observed that the enabling effect was increased by the lower doses of dexamethasone (Fig. 6C). Addition of other steroids such as estradiol 17β had no effect on enabling (Fig. 6D).

DISCUSSION

Here our analysis of DCIS cells that express only a single isoform of AIB1, AIB1Δ4, reveals a new 'enabler' function during the malignant progression of early stage breast cancer. Small subpopulations of cells, in an early stage tumor, gain expression of the AIB1Δ4 isoform that binds to distinct genomic engagement sites. This leads to significant differences in the distribution of H3K27ac that becomes more engaged at distinct breast cancer enhancer sites (41). The changes in the gene expression pattern in AIB1Δ4 cells are related to increased

inflammatory and 1q21.3 gene expression as well as factors that regulate the ECM. We propose that these changes in enabler gene expression drive crosstalk with responder cells increasing their WNT and NFκB signaling driving invasion and subsequent metastasis. It is of note that changes in WNT signaling through subpopulation cross talk has been observed previously in lung adenocarcinoma (51).

The GR and PPAR pathways appear to play a significant role in the enabler effect as evidenced by AIB1Δ4 engagement patterns, immune and PPAR related gene expression changes, and the ability of a GR or PPAR agonist to modulate the enabler effect. The GR plays diverse roles in breast cancer but is known to be involved in invasion and metastasis (52). Since AIB1 and AIB1Δ4 are both engaged at GREs in DCIS cells it seems likely that potential differences in transcriptional effects may be mediated by different patterns or strength of genomic engagement, and/or selective interactions with other coactivators and repressors at these sites. Likewise the selective engagement of AIB1Δ4 at PPARE elements is of interest since anti-inflammatory pathways are known to be down regulated by PPAR signaling pathways (50,53). The inhibitory effect of efatutazone indicates that PPARγ is involved in the enabling crosstalk. AIB1Δ4 could repress PPAR mediated transcription by selective recruitment of corepressors or may simply be a less-efficient coactivator at PPAR sites than AIB1 full length. Future experiments will tease out these possibilities and determine the components of the AIB1Δ4 transcription complex at GR, PPAR and other genomic engagement sites.

The increased activation by AIB1Δ4 of genes at the 1q21.3 locus is a component of the differences in inflammatory signaling. We have previously published an inhibitory role for full length AIB1 at the 1q21.3 locus where it binds ANCO1, a tumor suppressor, at TEAD binding sites to repress expression of SPRR and S100A genes (54). Amplification of the 1q21.3 locus in breast cancer patients is associated with an increased risk of recurrence and early relapse (55). AIB1Δ4 does not bind ANCO1(21) and is not repressed by this tumor suppressor suggesting that AIB1Δ4 can activate the 1q21.3 locus by-passing ANCO1 repression. The combination of effects of AIB1Δ4 at this locus as well as on GR and PPAR sites is a plausible explanation of the observed increases in inflammatory signaling that likely contributes to the enabling phenotype, tumor invasion and progression.

An unexpected aspect of AIB1Δ4 expression in DCIS is the slower growth *in vivo*. One explanation is that AIB1Δ4 lacks the N-terminal domain and is unable to interact with E2F in contrast to full length AIB1 (56) that drives expression of cell cycle genes such as cyclin D (57). Whatever the mechanism of slower growth, the enabling effect of the AIB1Δ4 isoform does not require increased proliferation. Indeed the slow proliferation of the AIB1Δ4 cells may well prevent them from being the selected dominant population in a tumor.

Overall, our observations raise the intriguing possibility that changes in splicing regulation increase expression of the AIB1Δ4 isoform in a subpopulation of cells and is responsible for initiating malignant progression. The detection of small populations of cells that express the AIB1Δ4 isoform could be predictive of DCIS lesions that are more aggressive and destined to metastasize. An AIB1Δ4 related gene expression signature in patients could also

be used to predict poor outcome. Future studies will determine if detection of changes in isoform expression patterns in early stage non-invasive breast cancer (DCIS) could indicate conversion to invasive cancer. In the longer term therapeutic targeting drivers of splicing or inhibition of enhancer activation by AIB1Δ4 could be useful in preventing the emergence of a small subpopulation enabling malignant progression of early stage disease.

Supplementary Material

Refer to Web version on PubMed Central for supplementary material.

Acknowledgements

We would like to thank our Georgetown University colleagues Dr Virginie Ory for contribution to the experiments as well as Drs Eric Glasgow and Matthew R Swift for their assistance in the zebrafish experiments. The project described used the Tissue Culture & Biobanking, Flow Cytometry & Cell Sorting, Microscopy & Imaging, Animal Model, Histopathology & Tissue, and Genomics & Epigenomics Shared Resources which are partially supported by Award Number P30CA051008 (PI: L.Weiner) from the National Cancer Institute. The content is solely the responsibility of the authors and does not necessarily represent the official views of the National Cancer Institute or the National Institutes of Health. Work was supported by NIH grants R01CA205632 (A.T. Riegel, A. Wellstein, G.M.Sharif, M.H.Kushner, W.B.Kietzman), R01CA218670 (G.W.Pearson, A. Nasir) and R21CA226542 (A.T. Riegel, G.M.Sharif, M.H.Kushner, W.B.Kietzman). NCI T32 CA009686 (G.T.Graham, M.H.Kushner, W.B.Kietzman), F31 CA232664 (M.H.Kushner).

REFERENCES:

1. Deslattes Mays A, Schmidt M, Graham G, Tseng E, Baybayan P, Sebra R, et al.Single-Molecule Real-Time (SMRT) Full-Length RNA-Sequencing Reveals Novel and Distinct mRNA Isoforms in Human Bone Marrow Cell Subpopulations. Genes (Basel). 2019;10.
2. Lee SC-W, Abdel-Wahab O. Therapeutic targeting of splicing in cancer. Nature Medicine. 2016;22:976–86.
3. Sendoel A, Dunn JG, Rodriguez EH, Naik S, Gomez NC, Hurwitz B, et al.Translation from unconventional 5' start sites drives tumour initiation. Nature. 2017;541:494–9. [PubMed: 28077873]
4. Trincado JL, Sebestyén E, Pagés A, Eyras E. The prognostic potential of alternative transcript isoforms across human tumors. Genome Med. 2016;8:85. [PubMed: 27535130]
5. Dehm SM, Schmidt LJ, Heemers HV, Vessella RL, Tindall DJ. Splicing of a novel androgen receptor exon generates a constitutively active androgen receptor that mediates prostate cancer therapy resistance. Cancer Research. 2008;68:5469–77. [PubMed: 18593950]
6. Anzick SL, Kononen J, Walker RL, Azorsa DO, Tanner MM, Guan XY, et al.AIB1, a steroid receptor coactivator amplified in breast and ovarian cancer. Science. 1997;277:965–8. [PubMed: 9252329]
7. Chen H, Lin RJ, Schiltz RL, Chakravarti D, Nash A, Nagy L, et al.Nuclear receptor coactivator ACTR is a novel histone acetyltransferase and forms a multimeric activation complex with P/CAF and CBP/p300. Cell. 1997;90:569–80. [PubMed: 9267036]
8. Torres-Arzayus MI, Font de Mora J, Yuan J, Vazquez F, Bronson R, Rue M, et al.High tumor incidence and activation of the PI3K/AKT pathway in transgenic mice define AIB1 as an oncogene. CCELL. 2004;6:263–74.
9. Dasgupta S, Rajapakshe K, Zhu B, Nikolai BC, Yi P, Putluri N, et al.Metabolic enzyme PFKFB4 activates transcriptional coactivator SRC-3 to drive breast cancer. Nature. 2018;556:249–54. [PubMed: 29615789]
10. Fereshteh MP, Tilli MT, Kim SE, Xu J, O'Malley BW, Wellstein A, et al.The Nuclear Receptor Coactivator Amplified in Breast Cancer-1 Is Required for Neu (ErbB2/HER2) Activation, Signaling, and Mammary Tumorigenesis in Mice. Cancer Research. 2008;68:3697–706. [PubMed: 18483252]

11. Lahusen T, Henke RT, Kagan BL, Wellstein A, Riegel AT. The role and regulation of the nuclear receptor co-activator AIB1 in breast cancer. Breast Cancer Res Treat. 2009;116:225–37. [PubMed: 19418218]
12. Ory V, Tassi E, Cavalli LR, Sharif GM, Saenz F, Baker T, et al.The nuclear coactivator amplified in breast cancer 1 maintainstumor-initiating cells during development of ductal carcinomain situ. Oncogene; 2013:1–10.
13. Torres-Arzayus MI, Yuan J, DellaGatta JL, Lane H, Kung AL, Brown M. Targeting the AIB1 oncogene through mammalian target of rapamycin inhibition in the mammary gland. Cancer Res. 2006;66:11381–8. [PubMed: 17145884]
14. Wu R-C, Qin J, Hashimoto Y, Wong J, Xu J, Tsai SY, et al.Regulation of SRC-3 (pCIP/ACTR/AIB-1/RAC-3/TRAM-1) Coactivator activity by I kappa B kinase. Mol Cell Biol. 2002;22:3549–61. [PubMed: 11971985]
15. York B, O'Malley BW. Steroid Receptor Coactivator (SRC) Family: Masters of Systems Biology. Journal of Biological Chemistry. 2010;285:38743–50.
16. Chien CD, Kirilyuk A, Li JV, Zhang W, Lahusen T, Schmidt MO, et al.Role of the Nuclear Receptor Coactivator AIB1-Δ4 Splice Variant in the Control of Gene Transcription. The Journal Of Biological Chemistry. ASBMB; 2011;286:26813–27.
17. Reiter R, Wellstein A, Riegel AT. An Isoform of the Coactivator AIB1 That Increases Hormone and Growth Factor Sensitivity Is Overexpressed in Breast Cancer. Journal of Biological Chemistry. 2001;276:39736–41.
18. Tilli MT, Reiter R, Oh AS, Henke RT, McDonnell K, Gallicano GI, et al.Overexpression of an N-terminally truncated isoform of the nuclear receptor coactivator amplified in breast cancer 1 leads to altered proliferation of mammary epithelial cells in transgenic mice. Molecular Endocrinology. 2005;19:644–56. [PubMed: 15550471]
19. Lahusen T, Fereshteh M, Oh A, Wellstein A, Riegel AT. Epidermal growth factor receptor tyrosine phosphorylation and signaling controlled by a nuclear receptor coactivator, amplified in breast cancer 1. Cancer Res. 2007;67:7256–65. [PubMed: 17671194]
20. Zhang AH, Yeung PL, Li CW, Tsai SC, Dinh GK, Wu XY, et al.Identification of a novel family of ankyrin repeats containing cofactors for p160 nuclear receptor coactivators. The Journal Of Biological Chemistry. 2004;279:33799–805. [PubMed: 15184363]
21. Garee JP, Chien CD, Li JV, Wellstein A, Riegel AT. Regulation of HER2 oncogene transcription by a multifunctional coactivator/corepressor complex. Molecular Endocrinology. 2014;28:846–59. [PubMed: 24678732]
22. Miller FR, Santner SJ, Tait L, Dawson PJ. MCF10DCIS.com xenograft model of human comedo ductal carcinoma in situ. J Natl Cancer Inst. 2000;92:1185–6.
23. Hu M, Yao J, Carroll DK, Weremowicz S, Chen H, Carrasco D, et al.Regulation of in situ to invasive breast carcinoma transition. Cancer Cell. 2008;13:394–406. [PubMed: 18455123]
24. Thike AA, Iqbal J, Cheok PY, Tse GM-K, Tan PH. Ductal carcinoma in situ associated with triple negative invasive breast cancer: evidence for a precursor–product relationship. Journal of Clinical Pathology. 2013;66:665–70. [PubMed: 23539741]
25. Kietzman W, Riegel AT, Ory V. Early-Stage Progression of Breast Cancer. Breast Cancer - From Biology to Medicine. Chapter 4. InTech; 2017. DOI: 10.5772/65633
26. Soule HD, Maloney TM, Wolman SR, Peterson WD, Brenz R, McGrath CM, et al.Isolation and characterization of a spontaneously immortalized human breast epithelial cell line, MCF-10. Cancer Res. 1990;50:6075–86. [PubMed: 1975513]
27. Debnath J, Muthuswamy SK, Brugge JS. Morphogenesis and oncogenesis of MCF-10A mammary epithelial acini grown in three-dimensional basement membrane cultures. Methods. 2003;30:256–68. [PubMed: 12798140]
28. Lin Y-N, Nasir A, Camacho S, Berry DL, Schmidt MO, Pearson GW, et al.Monitoring Cancer Cell Invasion and T-Cell Cytotoxicity in 3D Culture. J Vis Exp. 2020.
29. Liao Y, Smyth GK, Shi W. featureCounts: an efficient general purpose program for assigning sequence reads to genomic features. Bioinformatics. 2014;30:923–30. [PubMed: 24227677]
30. Lun ATL, Smyth GK. csaw: a Bioconductor package for differential binding analysis of ChIP-seq data using sliding windows. Nucleic Acids Research. 2016;44:e45. [PubMed: 26578583]

31. Heinz S, Benner C, Spann N, Bertolino E, Lin YC, Laslo P, et al.Simple combinations of lineage-determining transcription factors prime cis-regulatory elements required for macrophage and B cell identities. Molecular Cell. 2010;38:576–89. [PubMed: 20513432]
32. Zwart W, Theodorou V, Kok M, Canisius S, Linn S, Carroll JS. Oestrogen receptor–co-factor–chromatin specificity in the transcriptional regulation of breast cancer. EMBO J. Nature Publishing Group; 2011;30:4764–76.
33. Loudig O, Milova E, Brandwein-Gensler M, Massimi A, Belbin TJ, Childs G, et al.Molecular restoration of archived transcriptional profiles by complementary-template reverse-transcription (CT-RT). Nucleic Acids Research. 2007;35:e94. [PubMed: 17636051]
34. Sharif GM, Schmidt MO, Yi C, Hu Z, Haddad BR, Glasgow E, et al.Cell growth density modulates cancer cell vascular invasion viaHippo pathway activity and CXCR2 signaling. Oncogene. Nature Publishing Group; 2015;:1–11.
35. Berens EB, Sharif GM, Schmidt MO, Yan G, Shuptrine CW, Weiner LM, et al.Keratin-associated protein 5–5 controls cytoskeletal function and cancer cell vascular invasion. Oncogene. 2017;36:593–605. [PubMed: 27375028]
36. Levental KR, Yu H, Kass L, Lakins JN, Egeblad M, Erler JT, et al.Matrix crosslinking forces tumor progression by enhancing integrin signaling. Cell. 2009;139:891–906. [PubMed: 19931152]
37. Cross LM, Cook MA, Lin S, Chen J-N, Rubinstein AL. Rapid analysis of angiogenesis drugs in a live fluorescent zebrafish assay. Arteriosclerosis, Thrombosis, and Vascular Biology. 2003;23:911–2.
38. Lodillinsky C, Infante E, Guichard A, eacute RC, Fuhrmann L, Cyrta J, et al.p63/MT1-MMP axis is required for in situ to invasive transition in basal-like breast cancer. Oncogene. Nature Publishing Group; 2015;35:344–57.
39. Creyghton MP, Cheng AW, Welstead GG, Kooistra T, Carey BW, Steine EJ, et al.Histone H3K27ac separates active from poised enhancers and predicts developmental state. Proceedings of the National Academy of Sciences. 2010;107:21931–6.
40. Heintzman ND, Stuart RK, Hon G, Fu Y, Ching CW, Hawkins RD, et al.Distinct and predictive chromatin signatures of transcriptional promoters and enhancers in the human genome. Nature Genetics. 2007;39:311–8. [PubMed: 17277777]
41. Patten DK, Corleone G, Györffy B, Perone Y, Slaven N, Barozzi I, et al.Enhancer mapping uncovers phenotypic heterogeneity and evolution in patients with luminal breast cancer. Nature Medicine. 2018;24:1469–80.
42. Lizio M, Harshbarger J, Shimoji H, Severin J, Kasukawa T, Sahin S, et al.Gateways to the FANTOM5 promoter level mammalian expression atlas. Genome Biol. 2015;16:22. [PubMed: 25723102]
43. Serysheva E, Berhane H, Grumolato L, Demir K, Balmer S, Bodak M, et al.Wnk kinases are positive regulators of canonical Wnt/b-catenin signalling. EMBO reports. Nature Publishing Group; 2013;14:718–25.
44. Serysheva E, Mlodzik M, Jenny A. WNKs in Wnt/β-catenin signaling. Cell Cycle. 2014;13:173–4. [PubMed: 24241206]
45. Jia Y, Zeng Z-Z, Markwart SM, Rockwood KF, Ignatoski KMW, Ethier SP, et al.Integrin fibronectin receptors in matrix metalloproteinase-1-dependent invasion by breast cancer and mammary epithelial cells. Cancer Res. 2004;64:8674–81. [PubMed: 15574776]
46. Wang X, Wang Y, Yu L, Sakakura K, Visus C, Schwab JH, et al.CSPG4 in cancer: multiple roles. Curr Mol Med. 2010;10:419–29. [PubMed: 20455858]
47. Wang S, Sun H, Ma J, Zang C, Wang C, Wang J, et al.Target analysis by integration of transcriptome and ChIP-seq data with BETA. Nature Protocols. Nature Publishing Group; 2019;:1–14.
48. Ory V, Kietzman WB, Boeckelman J, Kallakury BV, Wellstein A, Furth PA, et al.The PPARγ agonist efatutazone delays invasive progression and induces differentiation of ductal carcinoma in situ. Breast Cancer Res Treat. 2018;169:47–57. [PubMed: 29350308]
49. Remels AHV, Langen RCJ, Gosker HR, Russell AP, Spaapen F, Voncken JW, et al.PPARγ inhibits NF-κB-dependent transcriptional activation in skeletal muscle. American Journal of Physiology-Endocrinology and Metabolism. 2009;297:E174–83. [PubMed: 19417127]

50. Straus DS, Glass CK. Anti-inflammatory actions of PPAR ligands: new insights on cellular and molecular mechanisms. Trends in Immunology. 2007;28:551–8. [PubMed: 17981503]

51. Tammela T, Sánchez-Rivera FJ, Cetinbas NM, Wu K, Joshi NS, Helenius K, et al.A Wnt-producing niche drives proliferative potential and progression in lung adenocarcinoma. Nature. Nature Publishing Group; 2017;545:355–9.

52. Obradović MMS, Hamelin B, Manevski N, Couto JP, Sethi A, Coissieux M-M, et al.Glucocorticoids promote breast cancer metastasis. Nature. Springer US; 2019;:1–25.

53. Zimmerman TL, Thevananther S, Ghose R, Burns AR, Karpen SJ. Nuclear export of retinoid X receptor alpha in response to interleukin-1beta-mediated cell signaling: roles for JNK and SER260. The Journal Of Biological Chemistry. 2006;281:15434–40. [PubMed: 16551633]

54. Kushner MH, Ory V, Graham GT, Sharif GM, Kietzman WB, Thevissen S, et al.Loss of ANCO1 repression at AIB1/YAP targets drives breast cancer progression. EMBO reports. 2020;21:1.

55. Goh JY, Feng M, Wang W, Oguz G, Yatim SMJM, Lee PL, et al.Chromosome 1q21.3 amplification is a trackable biomarker and actionable target for breast cancer recurrence. Nature Medicine. 2017;23:1319–30.

56. Louie MC, Zou JX, Rabinovich A, Chen H-W. ACTR/AIB1 functions as an E2F1 coactivator to promote breast cancer cell proliferation and antiestrogen resistance. Mol Cell Biol. 2004;24:5157–71. [PubMed: 15169882]

57. Nakles RE, Shiffert MT, Díaz-Cruz ES, Cabrera MC, Alotaiby M, Miermont AM, et al.Altered AIB1 or AIB1Δ3 expression impacts ERα effects on mammary gland stromal and epithelial content. Mol Endocrinol. 2011;25:549–63. [PubMed: 21292825]

SIGNIFICANCE

A minor subset of early stage breast cancer cells expressing AIB1Δ4 enables bulk tumor cells to become invasive, suggesting that selective eradication of this population could impair breast cancer metastasis.

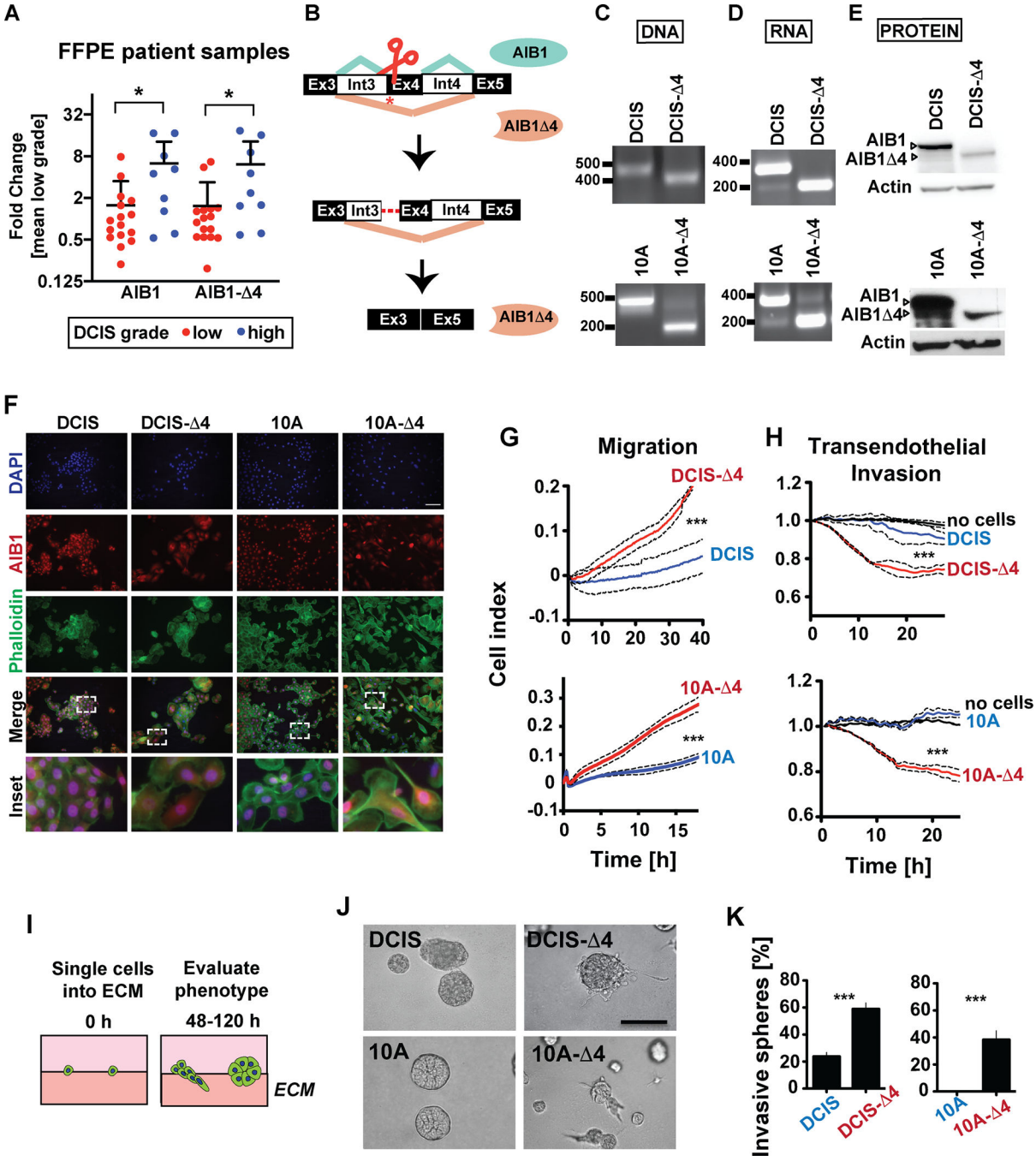

Figure 1. The AIB1Δ4 splice variant enhances cell motility and invasion.

A) qPCR of AIB1 and AIB1Δ4 on FFPE breast Ductal Carcinoma *in situ* (DCIS) samples of either low or high grade DCIS stage. *p<0.05. Fold changes are relative to the mean expression in low grade DCIS samples. Total of 25 samples were analyzed, 10 of which were ER-negative.

B) Schematic of AIB1 pre-mRNA alternative splicing that results in either AIB1(green) or AIB1Δ4 (orange). The asterisk denotes the gRNA target sequence on exon 4. CRISPR partial deletion of intron 3 and exon 4 (dotted line). Ex: exon, Int: intron.

C) Genomic DNA spanning exon 4 in the cell lines that were transfected with CRISPR-Cas9 and gRNA targeting AIB1 exon 4 splice junction.
D) AIB1 mRNA between exon 2 and exon 5 in the AIB1Δ4 cell lines and the parental control cells. Loss of exon 4 also confirmed by Sanger sequencing in Fig. S1B.
E) AIB1 isoforms' protein level in AIB1Δ4 cell lines and the parental cells. Isoforms indicated by arrowheads. Actin serves as a loading control.
F) Immunofluorescent staining of AIB1 isoforms, nucleus (dapi), actin cytoskeleton (Phalloidin) show cell morphology and nuclear localization of both AIB1 isoforms. Scale bar = 50μm.
G) Transwell migration assay using Electric Cell Impedance Sensing (ECIS) to monitor cell motility across a porous membrane. ***p<0.001. See Fig. S1E for assay schematic.
H) Invasion assay of AIB1Δ4 and control cells invading through an endothelial monolayer monitored by ECIS. No cells added to the endothelial cells as a negative control. ***p<0.001. See Fig. S1E for assay schematic.
I) A schematic of the single cell sphere formation assay in 100% matrigel.
J) Representative images of 3D spheres in 100% matrigel from single cell suspension of MCFDCIS at day 5 and MCF10A at day 3. Scale bar = 200μm.
K) The percentage of invasive spheres with protruding cells relative to the total spheres. Error bars indicate mean ±SD. Total number of spheres ~200 per condition. ***p<0.001.

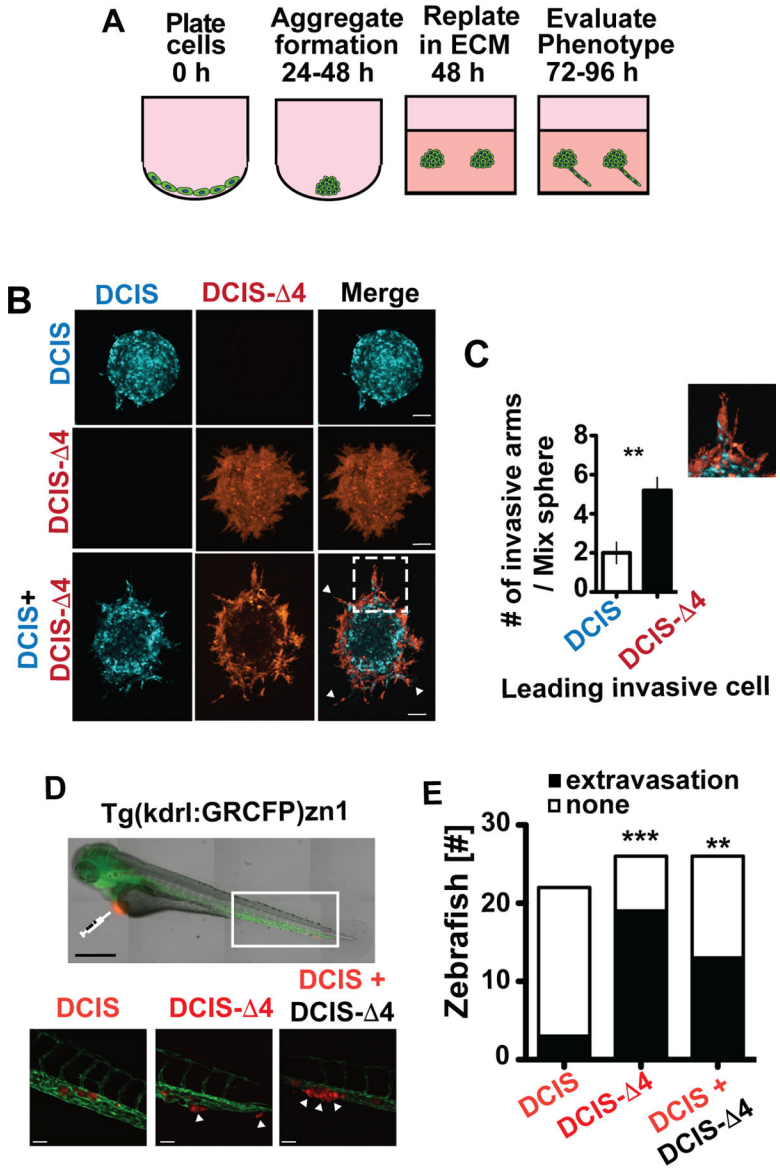

Figure 2. Direct contact with AIB1Δ4 expressing cells enables crosstalk and invasion.

A) A schematic of the cell aggregate invasion assay in 80% collagen I and 20% matrigel.

B) Representative images of cell aggregates of DCIS (blue), DCIS-Δ4 (red) or a 4:1 mix (DCIS:DCIS-Δ4) in collagen I and matrigel mix. Scale bar = 50μm.

C) Frequency of DCIS or DCIS-Δ4 at the leading edge in mixed spheres. n=5 **p<0.01. Inset: Magnified image from mixed spheres that shows DCIS-Δ4 cells leading the stream of invasive cells.

D) Extravasation of DCIS, DCIS-Δ4 or mixed cells in Tg(flk-1:GFP) transgenic zebrafish embryos. Scale bar = 500μm on whole fish, 50μm on tail images. White arrow heads point to extravasated cells.

E) The number of Zebrafish embryos with DCIS, DCIS- Δ4 or mixed cells that have extravasated out of the blood vessels and into the neighboring tissue. In the mixed cell

population, only DCIS parental line was fluorescently labeled and scored for extravasation. DCIS and DCIS- Δ4 are mixed at a 4:1 ratio. **p<0.01, ***p<0.001.

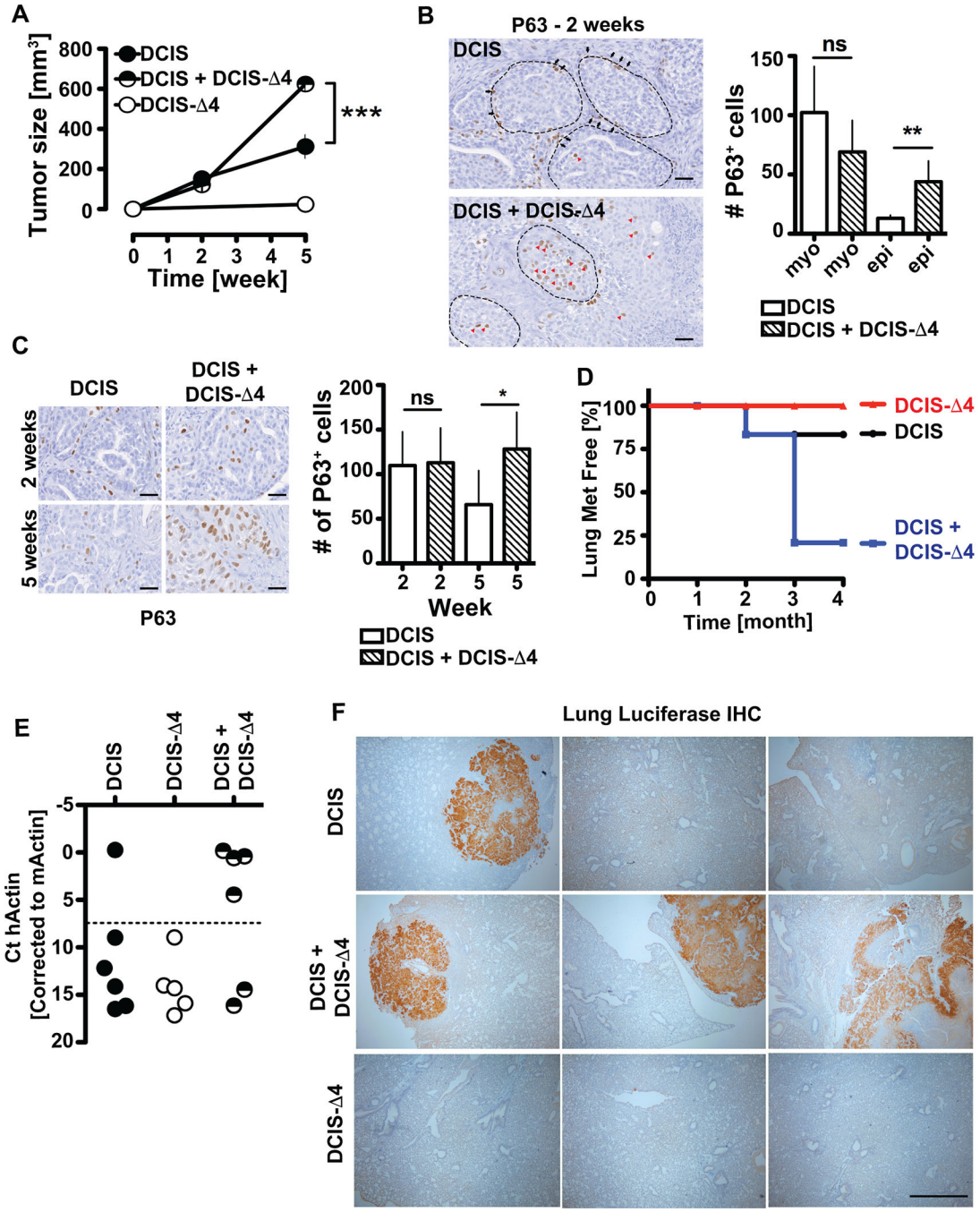

Figure 3. Indolent AIB1Δ4 cells *in vivo* are enabler of invasion and metastasis.

A) Growth of xenograft tumors from DCIS, DCIS-Δ4 or a mix of the two cell populations (4:1 respectively) injected in MFP of SCID/Beige mice. n=6 ***p<0.001

B) Representative images of P63 staining of xenografts from A at 2 weeks. Red arrowheads indicate luminal epithelial cells (epi) and black arrows indicate peripheral myoepithelial (myo) that are P63 positive. Black dotted line outlines *in situ* lesions. Graph showing the mean ± SD of P63 positive cells. Three 10x fields of 6 tumors were counted per group. **p<0.01. Scale bar = 50μm.

C) Representative images of P63 staining of xenografts from A. Graph showing the mean ± SD of P63 positive cells (nuclei). Five 20x fields of 6 tumors were counted per group. Scale bar = 50μm.

D) Lung metastases from primary MFP xenografts occurrence over time.

E) qPCR for human actin in lung tissues from fig. 3D. IVIS and histology were used to confirm lung metastases in samples with measurements above the dotted line.

F) Representative images of luciferase IHC of lung metastases from primary MFP xenografts. Signal is detected from parental DCIS harboring a luciferase construct, as opposed to the DCIS-Δ4 cells that are luciferase negative in the mix tumors. Scale bar = 500μm.

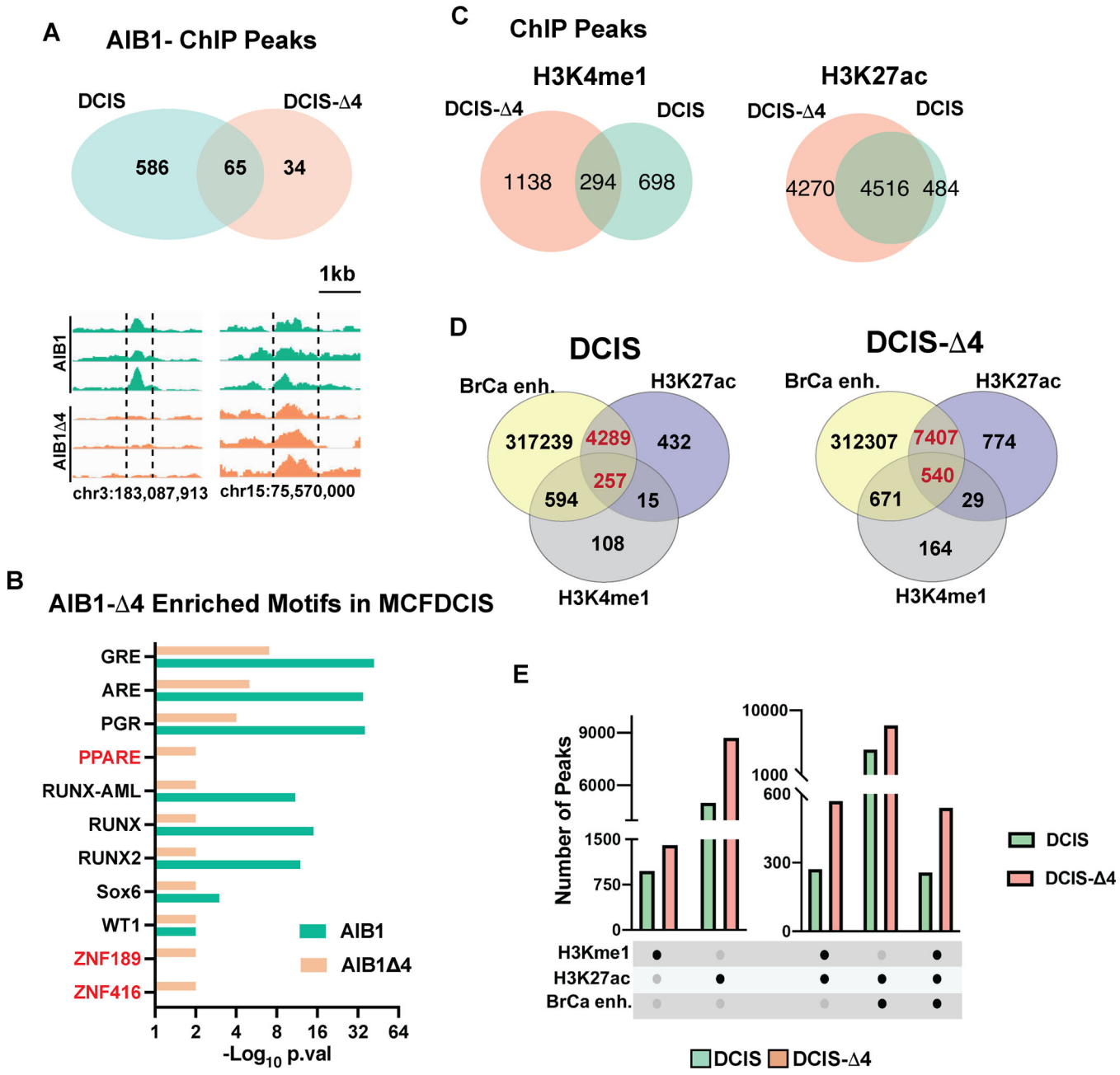

Figure 4: Differential genomic engagement of the AIB1Δ4 isoform impacts enhancer accessibility.

A) FDR-corrected shared and unique ChIP-Seq peaks for AIB1 and AIB1Δ4 in DCIS parental cell line and DCIS-Δ4, analyzed in biological triplicates, were compared for overlap (minimum 1bp) and uniqueness. Examples of unique and shared peak binding are illustrated on Chr 3 and Chr 15.

B) Motifs within 200 bp of the peak summit for significant ChIP-Seq peaks were analyzed for motif enrichment using HOMER. In red are those unique to AIB1Δ4 in MCFDCIS cells.

C) FDR-corrected shared and unique ChIP-Seq peaks for H3K4me1 or H3K27ac in DCIS vs DCIS-Δ4. Shared peaks have at least 1bp overlap.

D) FDR-corrected shared and unique ChIP-Seq peaks for H3K4me1 or H3K27ac identified in either DCIS vs DCIS-Δ4 were overlapped with BrCa enhancers (BrCa enh) within a distance of 500 bp (41) Histone modification peaks in DCIS and DCIS-Δ4 overlapping with enhancer sites identified in breast cancer patients (BrCa enh).

E) The number of H3K27ac or H3K4me1 ChIP peaks and their overlap with BrCa enhancers (BrCa enh) in DCIS vs DCIS-Δ4.

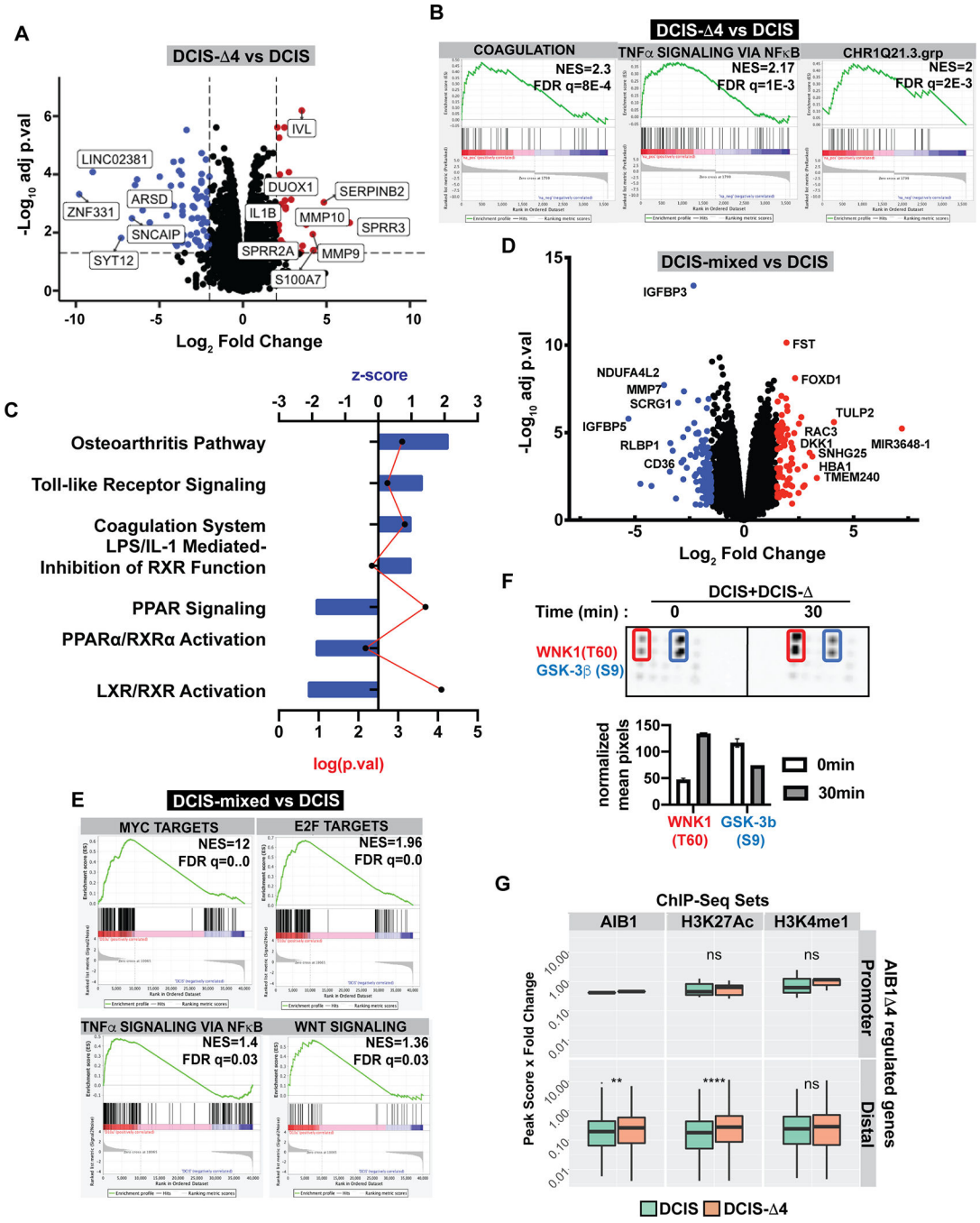

Figure 5. The AIB1Δ4 splice variant regulates different transcriptomes

A) Differentially expressed genes (DEGs) regulated by AIB1Δ4 in MCFDCIS cell clones (|log2(FC)|>1.5 and –log(adj p-val)>1.3). Full list of DEGs in supplementary table S1.

B) Gene set enrichment analyses (GSEA) associated with AIB1Δ4 expression in MCFDCIS cells. Full list of enriched pathways in supplementary table S2.

C) Top canonical pathways altered in MCFDCIS-Δ4 compared to control MFCFDCIS cells identified by Ingenuity Pathway Analysis (IPA). |z-score|>1, p-val <0.05.

D) Differentially expressed genes (DEGs) in MCFDCIS co-cultured with MCFDCIS-Δ4 compared to MCFDCIS alone. Mixed cells were then separated by flow cytometry prior to RNA-seq analysis. (|log2(FC)|>1.5 and –log(adj p-val)>1.3). Full list of DEGs in supplementary table S1.

E) Gene set enrichment analyses (GSEA) associated with mixed MCFDCIS cells compared to MCFDCIS alone. Full list of hallmark pathways in supplementary table S2.

F) A phospho-kinase profiler array shows change in phosphorylation of WNK1(T60) and GSK-3β(S9) in MCFDCIS cells after 30min of co-culture with MCFDCIS-Δ4. Graph shows quantification of normalized signal.

G) FDR-corrected ChIP-Seq peaks for AIB1, H3K4me1 or H3K27ac in either MCFDCIS or MCFDCIS-Δ4 cells were annotated to genes within 100 kb and filtered to those that were significantly regulated between the two cell types. For each significantly regulated gene the absolute fold change was multiplied by the sum of peak binding, either within promoter regions (within the body of the gene, and 2.5kb of either the TSS or TTS) of distal regions (47). The median top 75^{th} and bottom 25^{th} percentiles are shown as a box-whisker plot. End points of the lines (whiskers) are at a distance of 1.5*IQR, where IQR: Inter Quartile Range is the distance between 25^{th} and 75^{th} percentiles. The extreme points outside the whiskers are marked as dots. Wilcox test determined significance. **p<0.01, ****p<0.0001. Promoter<2.5kb, 2.5kb<Distal<50kb.

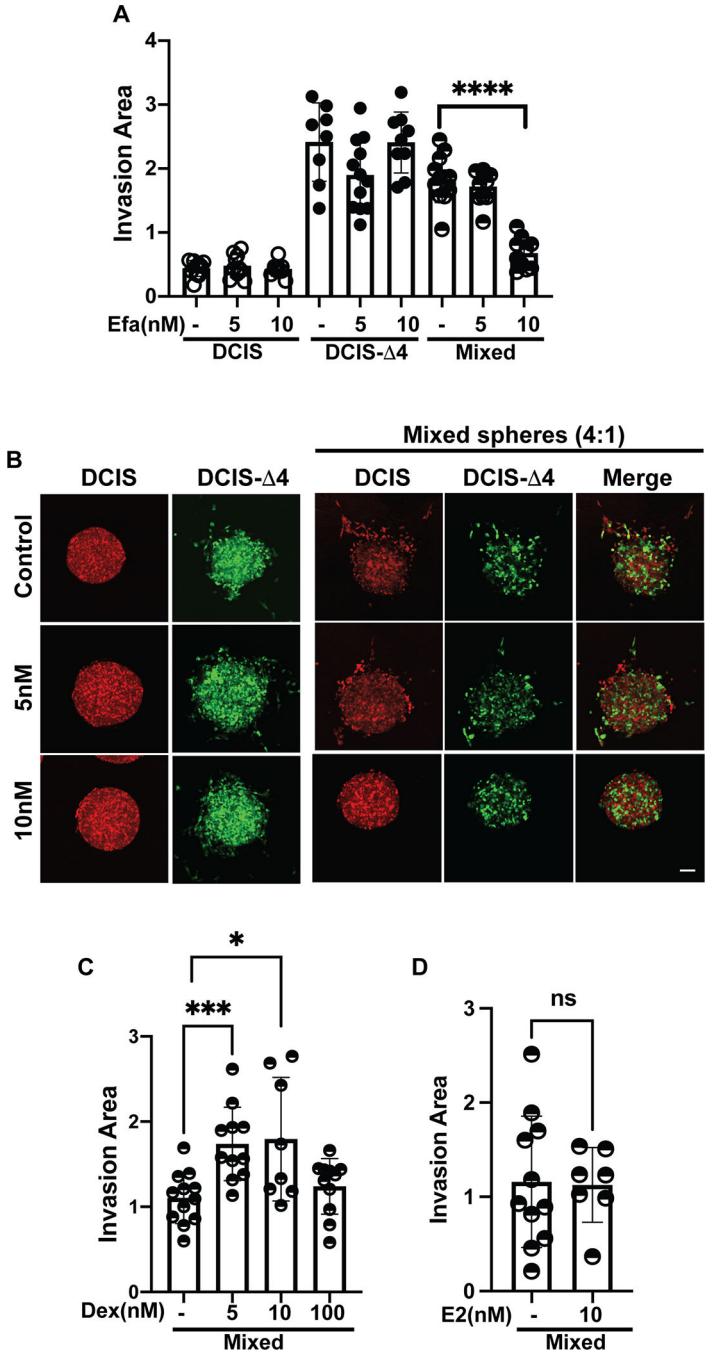

Figure 6: Blocking the enabler effect of AIB1Δ4 by activating PPARγ signaling pathway.

A) DCIS, DCIS-Δ4 or a 4:1 mix (DCIS:DCIS-Δ4) 3D sphere invasion in 80% collagen I and 20% matrigel treated with the indicated doses of efatutazone (Efa) or DMSO as a control (−). ****p<0.0001

B) Representative images of 3D invasion from fig. 6A.

C) Invasion of mixed spheres treated with dexamethasone (Dex) or DMSO control (−). *p<0.05, ***p<0.001.

D) Invasion of mixed spheres treated with Estradiol (E2) or ethanol control (−). ns: not significant.